Mesoscopic Free Path of Nonthermalized Photogenerated Carriers in a Ferroelectric Insulator

Zongquan Gu, Dominic Imbrenda, Andrew L. Bennett-Jackson, Matthias Falmbigl, Adrian Podpirka, Thomas C. Parker, Daniel Shreiber, Mathew P. Ivill, Vladimir M. Fridkin, and Jonathan E. Spanier

Phys. Rev. Lett. **118**, 096601 — Published 1 March 2017

DOI: 10.1103/PhysRevLett.118.096601

Mesoscopic free path of non-thermalized photogenerated carriers in a ferroelectric insulator

Zongquan Gu* and Dominic Imbrenda*
Department of Electrical & Computer Engineering, Drexel University, Philadelphia, PA 19104, USA

Andrew L. Bennett-Jackson, Matthias Falmbigl, and Adrian Podpirka
Department of Materials Science & Engineering, Drexel University, Philadelphia, PA 19104, USA

Thomas C. Parker, Daniel Shreiber, and Mathew P. Ivill
US Army Research Laboratory, Aberdeen Proving Ground, MD 21005, USA

Vladimir M. Fridkin†
Shubnikov Institute of Crystallography, Russian Academy of Sciences, Leninsky Prospect 59, Moscow, 117333, Russian Federation

Jonathan E. Spanier‡
Department of Materials Science & Engineering, Drexel University, Philadelphia, PA 19104, USA

(Dated: February 2, 2017)

We show how finite-size scaling of bulk photovoltaic effect-generated electric field in epitaxial ferroelectric insulating $BaTiO_3$(001) films and photo-Hall response involving the bulk photovoltaic current reveal large room-temperature mean free path of photogenerated non-thermalized electrons. Experimental determination of mesoscopic ballistic optically generated carrier transport opens a new paradigm for hot electron-based solar energy conversion, and for facile control of ballistic transport distinct from existing low-dimensional semiconductor interfaces, surfaces, layers or other structures.

Ballistic transport of carriers is a celebrated feature of selected two- and one-dimensional systems [1–6] in which mean free path is limited by scattering by other carriers, defects, and phonons. In band insulators, however, such transport is impossible within the material bulk, even in crystals of exceptional quality. The bulk photovoltaic effect in crystals without a center of symmetry [7–11] is caused by asymmetric distribution of non-thermalized carrier momentum, a consequence of the violation of the Boltzmann principle of detailed balance [10], and is analogous to parity non-conservation in the weak interaction [12]. Long after the discoveries of remarkably large photovoltages in SbSI [7] and in $LiNbO_3$ [8], photovoltaic effects in ferroelectrics continue to attract renewed attention [11, 13–23]. While photovoltages in ferroelectrics can greatly exceed the band gap, the direct conversion of light energy to electricity has been extremely low until recently [14, 22, 23]. Carrier separation and photo-generated current collection in ferroelectrics can arise in principle from several effects, including spatial variation in electrostatic potential due to interfaces or interfacial regions, *e.g.*, domain walls and/or space-charge at and near the ferroelectric-metal interface, transient responses due to pyroelectric and depolarizing field effects, and effects caused by inhomogeneous illumination. In conventional solar cells collection of photogenerated carriers is bounded by their diffusion length. In the bulk photovoltaic effect, however, knowledge of the free path of hot electrons in such states is paramount to understanding and improving conversion efficiency.

The bulk photovoltaic effect (BPE) involving spatially homogenous illumination in crystals lacking centre of inversion symmetry exists even in the absence of these aforementioned effects. The BPE and the resulting separation of photogenerated electrons and holes have been explained by two possible mechanisms, ballistic and shift. The ballistic mechanism is associated with excitation of non-thermalized (hot) carriers in a non-centrosymmetric crystal, leading to an asymmetric distribution of non-thermalized carrier momentum and a violation of the Boltzmann principle of detailed balance [10]. In the ballistic mechanism the photoexcited non-thermalized carriers lose their energy and descend to the bottom of the conduction band over a free path, *i.e.*, thermalization length, l_0. Shift current, the alternative mechanism for the BPE, is obtained by accounting for the non-diagonal elements of the density matrix [9], established within the framework of density functional theory [11, 24]. One interpretation of this shift mechanism shows that, in spite of coexistence of the two mechanisms, shift current evolution does not involve inertia [10]. On the contrary, the ballistic current is caused by free carrier transport and contributes to the (photo)-Hall effect. Nevertheless, both mechanisms can contribute to the BPE.

In the bulk crystal the power conversion efficiency via the BPE is extremely small, *i.e.*, 10^{-5}-10^{-6}. It was shown that in nanoscale-thickness $BaTiO_3$ films, the internal power conversion efficiency (under monochromatic illumination, $\lambda = 360$ nm) is enhanced by more than four orders of magnitude, to $\lesssim 1\%$ [23]. This finite size effect can be explained phenomenologically in terms of the ballistic mechanism.

The tensor properties of the linear BPE current are described [10] by

$$J_i = G^L_{ijl} e_j e^*_l I + i G^C_{il} [e e^*]_i I \tag{1}$$

where e_j and e_l are components of the light polarization vector and G^L_{ijl} is the corresponding third-rank tensor (for point group C_{4v} of $BaTiO_3$) and I is the incident light intensity. (G^C_{il} is a second rank tensor relevant for gyrotropic materials.) For unpolarized radiation, the first term of Eq. (1) can be written in its scalar form $j_{pv} = G_{31} I = \alpha g_{31} I$ where α is the $BaTiO_3$ film absorption coefficient for $\hbar\omega \approx 3$ eV ($\alpha \approx 150$ cm^{-1}).

The field E_{pv} generated by current j is given by $E_{pv} = j/\sigma_{ph}$ where $\sigma_{ph} = e\varphi\alpha I(\hbar\omega)^{-1}(\mu\tau)$ is the photoconductivity. Here e is the elementary charge, $\varphi \leq 1$ is the quantum yield, $\hbar\omega$ is the quantum of energy and μ and τ are the mobility and lifetime of non-equilibrium carriers, respectively. Thus the field generated by the BPE current is

$$E_{pv} = \frac{g_{31}\hbar\omega}{e\varphi(\mu\tau)}. \tag{2}$$

It is seen from Eq. (2) that the finite-size effect on E_{pv} and on internal power conversion efficiency ($= g_{31}E_{pv}/4$) [10, 23] is caused by the thermalization. Following thermalization the hot electrons become (thermalized) polarons, which do not contribute to the BPE due to their symmetric momentum distribution. The finite-size effect is related to $(\mu\tau)_{nt} \ll (\mu\tau)_t$, where $(\mu\tau)_{nt}$ and $(\mu\tau)_t$ are the mobility-lifetime products for non-thermalized and thermalized electrons, respectively, and, correspondingly, $E^t_{pv} \ll E^{nt}_{pv}$. Simultaneously internal power conversion efficiency strongly decreases for $l \gg l_0$.

The ballistic theory of BPE for excitation from donors within a dipole-impurity model yields for the ballistic current [10, 25] $j^{bal} = e\varphi\alpha I(\hbar\omega)^{-1} l_0 \xi$, where l_0 is the free path of non-thermalized electrons (Fig. 1*a*) and $\xi = \xi(\hbar\omega)$ is a microscopic parameter that characterizes the asymmetry of the photo-excited electron momentum distribution. A dipole-impurity model for $k_0 a \simeq 1$ suggests that ξ will not exceed $\xi_{max} = 0.1$ [10, 25] where k_0 is momentum and a is the lattice constant (for $BaTiO_3$ $a \approx 0.4$ nm).

The ballistic nature of photo-generated electrons in ferroelectric $BaTiO_3$ is confirmed by a Hall mobility measurement of non-thermalized electrons in a single crystal (Fig. 1*c,d*) under illumination along [001] at 300 K. Photovoltaic current density j_z was collected along [001] at several values of applied electric field E and no magnetic field ($B = 0$) using semi-transparent electrodes, yielding $g_{31} = 2 \times 10^{-8}$ cm/V, in agreement with earlier work [23], with short-circuit current density $j_{z0} = 1.0{\times}10^{-11}$ A/cm^2. Application of magnetic field $B = 1.4$ T along [010] produced a Hall component $j_x = 2.7{\times}10^{-12}$ A/cm^2. The mobility of non-thermalized electrons in the BPE regime [10] $\mu_{nt} = (1/B)(j_x/j_z) \approx$ 1,900 cm^2 V^{-1} s^{-1}, [14] three orders of magnitude larger than that for thermalized carriers, and demonstrating that the BPE in $BaTiO_3$ under 3 eV illumination is caused by ballistic transport [26]. Significantly this room-temperature value for μ_{nt} is also 1-2 orders of magnitude higher than the highest room-temperature carrier mobility reported for any complex oxide interface [4], surface [27] or bulk [28]. This permits us to get a rough estimate of l_0 for $BaTiO_3$. From the above, $g_{31} = e\varphi(\hbar\omega)^{-1}l_0\xi$. The values of tensor component $G_{31}(= \alpha g_{31})$ are known for many ferro- and piezoelectrics [10]. Substituting for $BaTiO_3$ $g_{31} \approx 10^{-8}$ cm V^{-1} and $\hbar\omega = 3$ eV one obtains $l_0 \approx 0.1(\varphi\xi)^{-1} \approx$ 10 - 100 nm.

Another estimate of l_0 can be obtained from the non-thermalized photo-Hall mobility of the ballistic electrons,

$$\mu_{nt} \simeq \frac{e}{m^*}\tau_{nt} \simeq \frac{el_0}{\bar{k}_0}, \tag{3}$$

where $k_0 a \simeq 1$. For $\mu_{nt} \simeq 1.9 \times 10^3$ cm^{2}V^{-1}sec^{-1} and $a \simeq 0.4$ nm

$$l_0 \simeq \frac{\hbar}{ea}\mu_{nt} \simeq 40 \text{ nm}. \tag{4}$$

We next describe the finite-size evolution of the BPE in single-domain $BaTiO_3$(001) epitaxial films ranging in thickness $8 \lesssim l \lesssim 900$ nm synthesized by pulsed laser deposition on $SrRuO_3$/$SrTiO_3$ (100) (Supplemental Material). Using $SrRuO_3$ and lithographically patterned indium tin oxide (ITO) films as planar bottom and top electrodes, respectively (Fig. 1*b*), $BaTiO_3$ films exhibited ferroelectric hysteresis (Supplemental Material) and were subsequently electrically poled along [001] with the $SrRuO_3$ bottom electrode held at a positive voltage with respect to the grounded ITO top electrode (*i.e.* polarization oriented upward). In accordance with tensor G at illumination along [001] for our geometry, E_{pv} is directed antiparallel to the direction of spontaneous polarization P, and the photovoltaic current flows in the same direction, [001]. Dependences of photovoltaic current on bias voltage were collected in each thin film under unpolarized monochromatic 3.06 eV illumination for a range of different incident intensities up to ≈ 0.18 W/cm^2, examples of which are shown in Fig. 2. Short-circuit current j_{sc} is linear with intensity (Fig. 3), yielding $g_{31} \approx 10^{-8}$ cm V^{-1}.

From the linear current density-voltage characteristic $j = j(V)$, thickness-dependent values of photovoltaic field $E_{pv}(l)$ $(= V/l)$ were obtained, showing a finite-size effect of $E_{pv} = E_{pv}(l)$ (Fig. 4*a*). E_{pv} increases from ≈ 170 V cm^{-1} in the 0.4 cm-thick crystal, which corresponds to the bulk value [10], approaching 10^5 V cm^{-1} for the 8, 14, 42 and 88 nm-thick films. Concomitantly internal power conversion efficiency increases by three orders of magnitude. It is seen from Fig. 4*a* that for $l \lesssim 100$ nm $E_{pv} \lesssim 10^5$ V cm^{-1}, *i.e.*, less than the Landau-Ginzburg intrinsic coercive field for $BaTiO_3$ ($\approx 10^8$ V cm^{-1}), accounting for the absence of switching in the nanoscale films by the BPE field. From the saturation value $E_{pv} \simeq 10^5$ V cm^{-1} and the above one can evaluate the lifetime of non-thermalized electrons τ_{nt}. Substituting $g_{31} \simeq 10^{-8}$ cm V^{-1}, $\mu_{nt} \simeq 10^3$ cm^{2}V^{-1}sec^{-1} and $\hbar\omega \simeq 3$ eV gives $\tau_{nt} \simeq 3 \times 10^{-13}\varphi^{-1}$ sec, which is in reasonable agreement with the typical relaxation time of nearly free electrons $\tau_{nt} = \mu_{nt}m/e \approx 10^{-12} - 10^{-14}$ sec [29].

Interestingly j_{sc} and g for the thinnest films drop two orders of magnitude within a single decade of thickness reduction (Fig. 4*b*). Simultaneously, E_{oc} remains essentially unchanged. Band bending in the thinnest films is likely present and is caused by the screening of spontaneous polarization. It is determined by the Debye screening length, which is on the order of $L_D \approx 10$ nm for insulating $BaTiO_3$ with a low concentration of carriers [30]. This bending at the surface leads to decrease of g (or of j_{sc}) as seen in Fig. 4b. But the generated field $E_{oc} = E_{pv} \approx \frac{j_{sc}}{\sigma_{ph}}$ remains essentially unchanged because the photoconductivity σ_{ph} is also decreased due to the volume screening charge and possible decrease of the lifetime. Our observation is presently limited by two experimental points in this thickness range, and it does not permit us to claim this conclusively. Nevertheless, the data in Fig. 4*a* indicate good agreement with the theoretically predicted value of the non-thermalized electron free path $l_0 \approx 100$ nm for 3 eV excitation. Clearly for shift current the induced field E_{pv} must also reveal the finite-size effect caused by thermalization of electrons which are responsible for photoconductivity. But the shift current itself does not involve carrier transport and for films with thicknesses comparable with the shift vector magnitude [11] the finite-size effect can be different.

In conclusion we have shown how the free path of photo-generated non-thermalized electrons can be determined experimentally, remarkably yielding a mesoscopic value which is in good agreement with theoretically predicted values,

for 3 eV. The non-equilibrium carriers, which are responsible for the ballistic photovoltaic current, have extremely high mobility. A new strategy for efficient photovoltaic solar energy conversion relies on hot carriers photo-generated within and collected from co-locating volumes of thermalization and screening in nanoscale electrode-interfaced ferroelectrics [13, 14]. An experimental prescription revealing an unexpectedly long room-temperature mean free path of photo-generated carriers in a ferroelectric insulator is key to advancing the promise of efficient bulk photovoltaic effect-based solar energy conversion.

Supplemental Material. Methods, X-ray diffraction, X-ray reflectivity, Rutherford backscattering spectroscopy, ferroelectric hysteresis, and film roughness data. [31]

---

* These authors contributed equally to this work.
† Also at Department of Physics, Drexel University, Philadelphia, PA 19104, USA
‡ Also at Department of Physics, and Department of Electrical & Computer Engineering, Drexel University, Philadelphia, PA 19104, USA; spanier@drexel.edu.

[1] T. Ando, A. B. Fowler, and F. Stern, Rev. Mod. Phys. **54**, 437 (1982).
[2] M. Bockrath, D. H. Cobden, P. L. McEuen, N. G. Chopra, A. Zettl, A. Thess, and R. E. Smalley, Science **275**, 1922 (1997).
[3] S. J. Tans, M. H. Devoret, H. Dai, A. Thess, R. E. Smalley, L. J. Geerligs, and C. Dekker, Nature **386**, 474 (1997).
[4] A. Ohtomo and H. Y. Hwang, Nature **427**, 423 (2004).
[5] K. S. Novoselov, A. K. Geim, S. V. Morozov, D. Jiang, M. I. Katsnelson, I. V. Grigorieva, S. V. Dubonos, and A. A. Firsov, Nature **438**, 197 (2005).
[6] Y. Zhang, Y. W. Tan, H. L. Stormer, and P. Kim, Nature **438**, 201 (2005).
[7] A. A. Grekov, M. A. Malitskaya, V. D. Spitsina, and V. M. Fridkin, Kristallografiya **15**, 500 (1970).
[8] A. M. Glass, D. von der Linde, and T. J. Negran, Appl. Phys. Lett. **25**, 233 (1974).
[9] R. von Baltz and W. Kraut, Phys. Rev. B **23**, 5590 (1981).
[10] B. Sturman and V. Fridkin, *The photovoltaic and photorefractive effects in noncentrosymmetric materials* (Gordon and Breach, Philadelphia, 1992).
[11] S. M. Young and A. M. Rappe, Phys. Rev. Lett. **109**, 116601 (2012), URL `http://link.aps.org/doi/10.1103/PhysRevLett.109.116601`.
[12] C. S. Wu, E. Ambler, R. W. Hayward, D. D. Hoppes, and R. P. Hudson, Phys. Rev. **105**, 1413 (1957).
[13] M. Alexe and D. Hesse, Nat. Commun. **2**, 256 (2011), URL `http://dx.doi.org/10.1038/ncomms1261`.
[14] J. E. Spanier, V. M. Fridkin, A. M. Rappe, A. R. Akbashev, A. Polemi, Z. Gu, Y. Qi, S. M. Young, D. Imbrenda, G. Xiao, et al., Nature Photon. **10**, 611 (2016), URL `http://dx.doi.org/10.1038/nphoton.2016.143`.
[15] S. Y. Yang, J. Seidel, S. J. Byrnes, P. Shafer, C. H. Yang, M. D. Rossell, P. Yu, Y. H. Chu, J. F. Scott, J. W. Ager, et al., Nat. Nanotech. **5**, 143 (2010), URL `http://dx.doi.org/10.1038/nnano.2009.451`.
[16] J. Seidel, D. Fu, S.-Y. Yang, E. Alarcón-Lladó, J. Wu, R. Ramesh, and J. W. Ager, Phys. Rev. Lett. **107**, 126805 (2011), URL `http://link.aps.org/doi/10.1103/PhysRevLett.107.126805`.
[17] J. Kreisel, M. Alexe, and P. A. Thomas, Nat. Mater. **11**, 260 (2012), URL `http://dx.doi.org/10.1038/nmat3282`.
[18] D. Daranciang, M. J. Highland, H. Wen, S. M. Young, N. C. Brandt, H. Y. Hwang, M. Vattilana, M. Nicoul, F. Quirin, J. Goodfellow, et al., Phys. Rev. Lett. **108**, 087601 (2012), URL `http://link.aps.org/doi/10.1103/PhysRevLett.108.087601`.
[19] I. Grinberg, D. V. West, M. Torres, G. Gou, D. M. Stein, L. Wu, G. Chen, E. M. Gallo, A. R. Akbashev, P. K. Davies, et al., Nature **503**, 509 (2013), URL `http://dx.doi.org/10.1038/nature12622`.
[20] V. Fridkin, IEEE Trans. Ultrason., Ferroelect., Freq. Control **60**, 1551 (2013), ISSN 0885-3010.
[21] A. Bhatnagar, A. Roy Chaudhuri, Y. Heon Kim, D. Hesse, and M. Alexe, Nat. Commun. **4** (2013), URL `http://dx.doi.org/10.1038/ncomms3835`.
[22] R. Nechache, C. Harnagea, S. Li, L. Cardenas, W. Huang, J. Chakrabartty, and F. Rosei, Nature Photon. **9**, 61 (2015), URL `http://dx.doi.org/10.1038/nphoton.2014.255`.
[23] A. Zenkevich, Y. Matveyev, K. Maksimova, R. Gaynutdinov, A. Tolstikhina, and V. Fridkin, Phys. Rev. B **90**, 161409 (2014), URL `http://link.aps.org/doi/10.1103/PhysRevB.90.161409`.
[24] S. M. Young, F. Zheng, and A. M. Rappe, Phys. Rev. Lett. **109**, 236601 (2012).
[25] V. Belinicher and B. Sturman, Sov. Phys. Usp. **23**, 199 (1980).
[26] S. Astafiev, V. Fridkin, V. Lazarev, and A. Shlensky, Ferroelectrics **83**, 3 (1988).
[27] J. Son, P. Moetakef, B. Jalan, B. O., N. J. Wright, R. Engel-Herbert, and S. Stemmer, Nat. Mater. **9**, 482 (2010).
[28] S. Raghavan, T. Schumann, H. Kim, J. Y. Zhang, T. A. Cain, and S. Stemmer, APL Materials **4**, 016106 (2016).
[29] C. Kittel, *Introduction to Solid State Physics* (John Wiley & Sons., New York, 1956).
[30] V. Fridkin, *Ferroelectric Semiconductors* (Consultants Bureau, New York, 1980).
[31] See Supplemental Material [url], which includes Refs. [32-33].
[32] M. Björck and G. Andersson, Journal of Applied Crystallography **40**, 1174 (2007).

[33] B. Jaffe, *Piezoelectric Ceramics*, vol. 3 (Academic Press, 1978).

Work supported by the US Army Research Office under grant no. W911NF-14-1-0500. Z.G. was supported by the National Science Foundation and the Semiconductor Research Corporation under the Nanoelectronics in 2020 and Beyond Program under grant no. DMR 1124696. M.F. was supported by the Office of Naval Research under grant no. N00014-1501102170. A.P. was supported by the SunShot Program of the US Department of Energy under grant no. DE-SC0014664. The research was partially sponsored by the Army Research Laboratory and was accomplished under Cooperative Agreement Number W911NF-12-2-0019. The authors acknowledge the Drexel core shared facilities and NSF DMR 1040166.

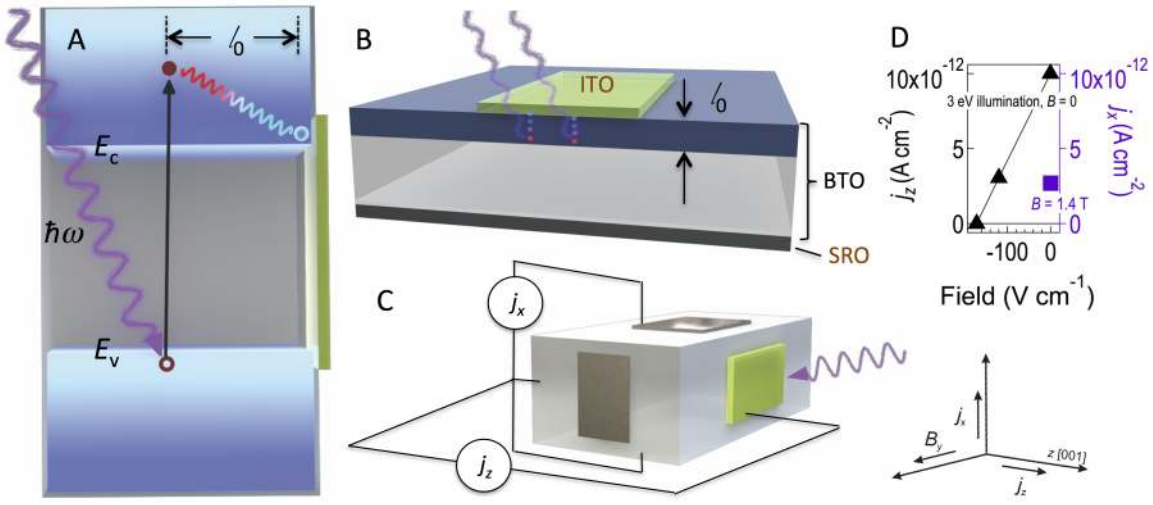

FIG. 1. **a**, Schematic band diagram illustrating the photo-excitation process in a non-centrosymmetric crystal depicting cooling of hot photogenerated bulk photovoltaic effect carriers collected only within a thermalization length l_0 of the contact. Illustration of experimental geometry of **b**, epitaxial BTO(001) film on an SRO bottom electrode used to determine thermalization length l_0 and **c**, photo-Hall measurements carried out on a bulk single crystal under 3 eV illumination exhibiting ballistic conduction in the ferroelectric insulator $BaTiO_3$ crystal at 300 K and **d**, current and photo-Hall current densities under zero and $B = 1.4$ T field.

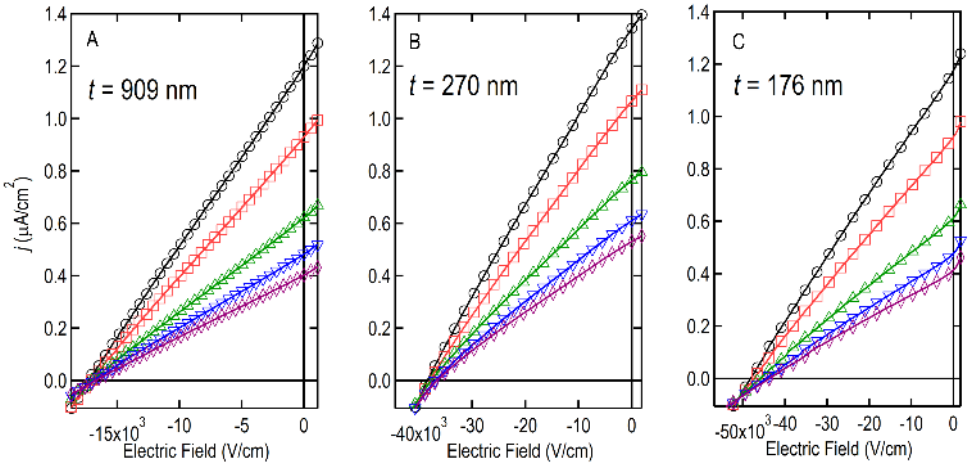

FIG. 2. Representative bulk photovoltaic responses in epitaxial $BaTiO_3$(001) films of thickness denoted in each panel. Films were deposited on $SrRuO_3$ film bottom electrodes on $SrTiO_3$(100) and responses measured under a range of intensities. The intensities in panels **a** and **b** are 0.182 (black circles), 0.145 (red squares), 0.101 (green triangles), 0.078 (blue triangles), and 0.067 (magenta diamonds) W/cm^2, and the intensities in **c** are 0.142 (black circles), 0.113 (red squares), 0.076 (green triangles), 0.060 (blue triangles) and 0.051 (magenta diamonds) W/cm^2 of monochromatic 3.06 eV (405 nm) illumination.

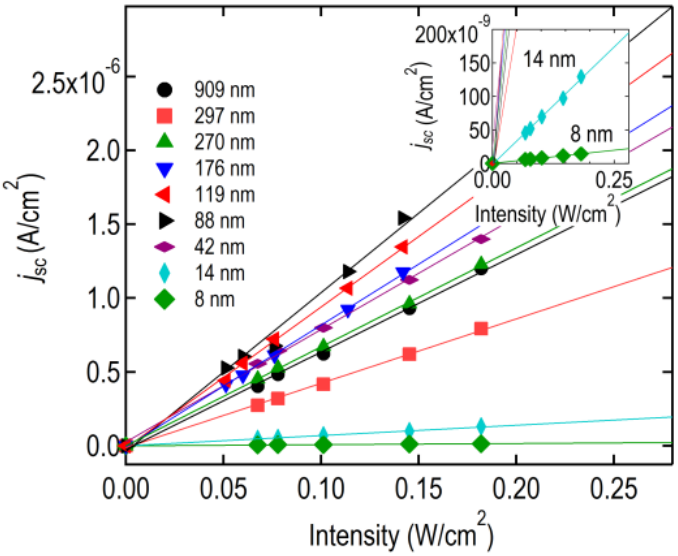

FIG. 3. Linear dependence of short circuit current j_{sc} on incident light intensity enabling determination of values of photovoltaic tensor component g_{31}. Plotted in the inset is an expanded range of current, showing data for the two thinnest films.

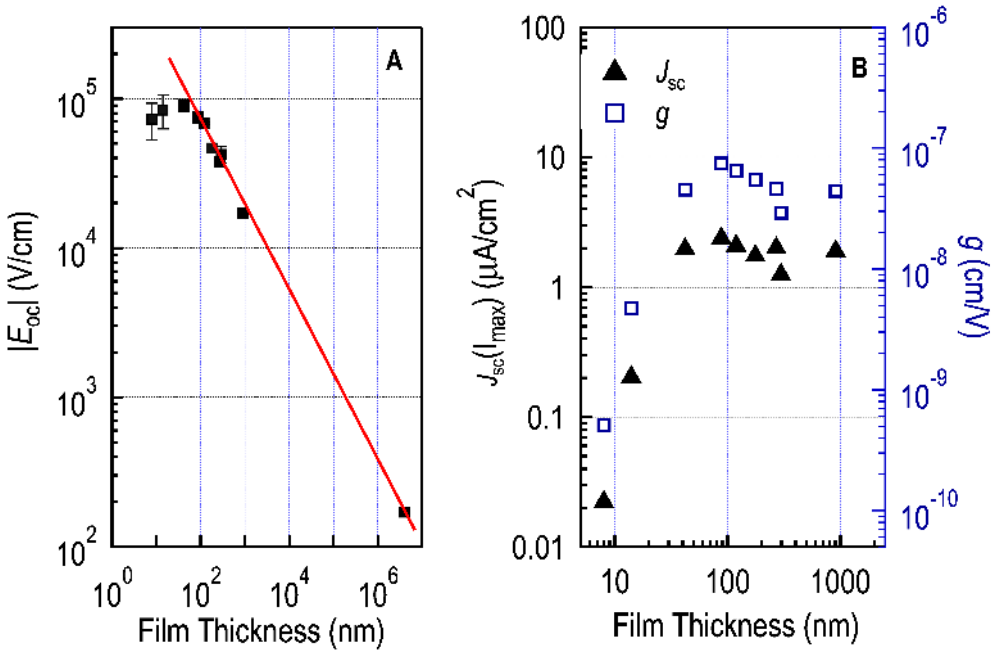

FIG. 4. **a**, Finite-thickness scaling of the magnitude of photovoltaic field $|E_{oc}(l)|$ in epitaxial single-domain $BaTiO_3$(001) films and a macroscopic $BaTiO_3$ crystal revealing onset of saturation for $l \approx 100$ nm and identification of scale of mean free path l_0 for $\hbar\omega \approx 3.1$ eV. The line is added as a guide to the eye, intersecting data points in a range over which the variation is clearly linear. **b**, Short-circuit current density j_{sc} and photovoltaic scalar g with thickness revealing a sharp decrease for thinner films.